

Iterative optical vector-matrix processor

M. Carlotto*

D. Casasent

Carnegie-Mellon University
Department of Electrical Engineering
Pittsburgh, Pennsylvania 15213

Abstract. An iterative optical vector-matrix processor capable of solving systems of linear algebraic equations or vector-matrix equations is described. The basic system uses a vector-matrix multiplier, consisting of a linear light emitting diode (LED) input array and fiber optic interconnections to a matrix mask interfaced to a linear output photodetector array. When the photodetector's outputs are returned to the LED inputs via a microprocessor electronic feedback system, an iterative optical processor results. The operation, description, and fabrication of this system are described, and its use as a rather general purpose optical processor is emphasized.

1. INTRODUCTION

In recent years, the flexibility of optical systems and the number of operations possible in an optical processor have increased remarkably.¹ Optical numerical processors using residue arithmetic^{2,4} and optical processors that operate on digital data⁵ have also been the subject of recent attention. In this paper, we consider an incoherent optical vector-matrix processor, specifically an iterative feedback version of one such system, as yet another class of flexible and general purpose optical processors. A wealth of pioneering work on optical vector-matrix and matrix-matrix processors exists.⁶⁻⁸ Researchers at the Naval Ocean Systems Center (NOSC)^{9,10} have fabricated a well-engineered system using a single light emitting diode (LED) light source whose output was time-sequentially modulated and used to illuminate a charge-coupled device (CCD) shift register detector through a fixed two-dimensional (2-D) mask. Stanford researchers¹¹ extended the concepts in Refs. 7-8 to a fully parallel, high-speed incoherent optical method for performing matrix-vector multiplications. They also extended this system to operate on bipolar¹² and complex-valued¹³ data and considered realization of the system using planar waveguides, fiber optics, and surface acoustic wave devices.¹⁴ The application they considered was the use of the matrix-vector multiplier to perform the discrete Fourier transform (DFT).¹¹ When the vector inputs are the time samples of the signal and the transmittances of the mask are proportional to the Fourier kernels, the output is the DFT of the input data.

In this paper, we describe the Carnegie-Mellon University (CMU) system.¹⁵ It is based upon the Stanford vector-matrix multiplier and the concepts in Ref. 7 with the addition of a microprocessor-controlled feedback system to provide an iterative optical vector-matrix processor that is capable of solving simultaneous linear equations, vector-matrix and matrix-matrix equations. We refer to this system as an iterative optical processor (IOP). In Sec. 2 the system architecture and the iterative algorithm realized on the IOP are described. In Sec. 3, we briefly describe how bipolar and complex-valued data can be handled on the system and describe a new technique used to handle such data on the IOP, including the necessary biasing, scaling, and post-processing using

the IOP's microprocessor support system. In Sec. 4, we describe the convergence of the iterative algorithm used and how convergence is insured on the laboratory IOP system. In Sec. 5 are discussed the fabrication details associated with the laboratory IOP system fabricated, including accuracy and its decreased size and weight. In Sec. 6 the operations possible on the IOP and several of its potential applications are summarized.

2. ITERATIVE ALGORITHM

In Fig. 1, we show a schematic of our original IOP¹⁵ modified to include an acceleration parameter ω (see Sec. 4) used both to insure convergence of the iterative algorithm and to speed its convergence. For the source array, we use a linear array of M light emitting diodes and describe their outputs at iteration j by the vector $\underline{a}^T(j)$, with elements $a_m(j)$. The outputs from P_1 of Fig. 1 are imaged vertically and expanded horizontally to uniformly illuminate the rows of a mask at P_2 . The transmittance of the mask is described by the $M \times N$ matrix \underline{B}^T , with elements B_{mn} . The light distribution leaving P_2 is integrated vertically and imaged horizontally onto a linear array of N photodetectors at P_3 . Its output $\underline{c}^T(j)$ is the vector-matrix product $\underline{a}^T(j)\underline{B}^T$. For notational simplicity, we will ignore the use of transposed matrices and vectors and describe the system's output at P_3 by

$$\underline{c}(j) = \underline{B}\underline{a}(j) \quad (1a)$$

or

$$c_n(j) = \sum_{m=1}^M a_m(j)b_{mn} \quad (1b)$$

Underlined lower-case and upper-case letters are used to denote vectors and matrices respectively. We will denote the arithmetic vector and matrix quantities by \underline{x} , \underline{y} , and \underline{H} and the optical system's physical inputs, outputs, and transmittances by \underline{a} , \underline{c} , \underline{B} . The elements a_m , c_n and b_{mn} of \underline{a} , \underline{c} and \underline{B} must be real and non-negative, whereas the elements of \underline{x} , \underline{y} , and \underline{H} need not be (see Sec. 3). Let us now describe how this basic vector-matrix multiplier can be used to produce an optical system capable of solving systems of

*Present address: The Analytic Sciences Corporation, 1 Jacob Way, Reading, MA 01867.

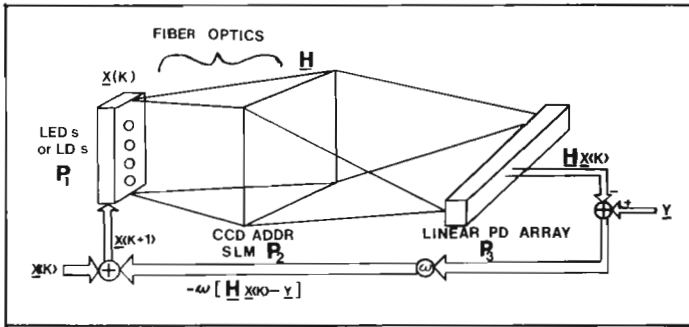


Fig. 1. Schematic diagram of an iterative optical processor (IOP).

linear algebraic equations or vector-matrix equations of the form $\underline{y} = \underline{H}\underline{x}$ for the unknown vector $\underline{x} = \underline{H}^{-1}\underline{y}$. To achieve this consider the input vector at iteration j at P_1 to be $\underline{x}(j)$ and the mask at P_2 to be \underline{H} . The difference between the photodetector outputs $\underline{H}\underline{x}(j)$ and a fixed external vector \underline{y} is formed, multiplied by ω , and added to the original $\underline{x}(j)$ to produce a new $\underline{x}(j+1)$ input. The system thus implements the Richardson algorithm,¹⁶

$$\underline{x}(j+1) = \underline{x}(j) + \omega[\underline{y} - \underline{H}\underline{x}(j)]. \quad (2)$$

When $\underline{x}(j) = \underline{x}(j+1) = \underline{x}$, Eq. (2) reduces to

$$\underline{y} = \underline{H}\underline{x} \quad (3)$$

and the system's output is thus the solution

$$\underline{x} = \underline{H}^{-1}\underline{y} \quad (4)$$

to the vector-matrix equation in Eq. (3).

3. BIPOLAR AND COMPLEX-VALUED DATA

The light distribution leaving the inputs at P_1 and the output from the detectors at P_3 must be real and nonnegative. Similarly, the transmittance of the masks at P_2 must be real and nonnegative. However, in many cases, the elements of the vectors and matrices to be processed will be bipolar or complex. In this section, we discuss how such data can be handled on the IOP. If the system could handle bipolar data, then complex-valued vectors and matrices could be handled by decomposing the vectors or matrices into their bipolar real (R) and imaginary (I) parts and using the system to realize

$$\begin{bmatrix} \underline{y}_R \\ \underline{y}_I \end{bmatrix} = \begin{bmatrix} \underline{H}_R & -\underline{H}_I \\ \underline{H}_I & \underline{H}_R \end{bmatrix} \begin{bmatrix} \underline{x}_R \\ \underline{x}_I \end{bmatrix}. \quad (5)$$

This can be achieved with an input array of $2M$ LEDs with the first M driven by \underline{x}_R and the second M driven by \underline{x}_I . The mask must now be of size $2M \times 2N$ and a $2N$ -element linear output photodetector array is required. To achieve the bipolar data necessary for Eq. (5), the input vectors and the matrix elements can all be biased such that their outputs and transmittances are positive. The photodetectors' outputs must then be postprocessed to extract \underline{y}_R and \underline{y}_I as described in Ref. 14.

To perform the necessary postprocessing requires the use of an additional row in the mask and an additional photodetector to obtain several of the bias terms necessary for the required postprocessing. In the current version of the IOP we are limited to small matrices ($M = N = 10$), and are concerned with the effect of fixed pattern detector and system noise on the accuracy of the

system. The increased space-bandwidth product required for the input array and moreover for the mask in the algorithm in Eq. (5) is, thus, not attractive. We therefore chose the alternative bipolar processing algorithm described below.

We decompose the input vector \underline{x} into its positive \underline{x}^+ and negative \underline{x}^- parts and as the optical system's input vectors we use the positive quantities

$$a_{1m} = 0.5(|x_m| + x_m) \quad (6a)$$

$$a_{2m} = 0.5(|x_m| - x_m), \quad (6b)$$

where a_{1m} and a_{2m} correspond to x_m^+ and x_m^- . For the optical mask, we scale and bias the matrix \underline{H} , such that the elements of \underline{B} are

$$b_{mn} = (h_{mn} - \underline{h})/(\bar{h} - \underline{h}), \quad (7)$$

where \underline{h} and \bar{h} are the minimum and maximum elements of \underline{H} . With Eq. (7), the elements of \underline{B} satisfy $0 \leq b_{mn} \leq 1$. We chose to achieve a bipolar vector-matrix multiplication in the IOP by operating the system twice, once with \underline{a}_1 as the input and once with \underline{a}_2 as the input (and with the same fixed $M \times N$ matrix mask \underline{B}). We formed the difference $\underline{B}\underline{a}_1 - \underline{B}\underline{a}_2$ between the system's outputs on the two cycles and scaled and biased this difference according to

$$\underline{y} = \underline{H}\underline{x} = (\bar{h} - \underline{h})[\underline{B}\underline{a}_1 - \underline{B}\underline{a}_2] + \underline{h} \sum_m x_m (1, \dots, 1)^T. \quad (8)$$

This reduces the system's throughput by a factor of two, but enables vectors and matrices of larger order to be processed. The algorithm in Eq. (8) is also quite attractive since it cancels fixed pattern detector noise, an error source we found to be of major concern (see Sec. 5).

In Fig. 2 the schematic diagram of the bipolar vector-matrix multiplier described by Eqs. (6) to (8) is shown. All of the multiplications and additions required are easily performed in dedicated hardware in the microprocessor feedback electronic support system. From here on, note we will not include the details in Fig. 2, but that they are necessary to handle bipolar data.

We next consider another method to handle complex-valued data on the IOP. A complex number \tilde{a} can be described by its three component projections along the 0° , 120° , and 240° axes in the complex plane by:

$$\tilde{a} = a_0 \exp(j0) + a_1 \exp(j2\pi/3) + a_2 \exp(j4\pi/3), \quad (9)$$

where a_0 , a_1 , and a_2 are real and positive. Many possible three-vector decompositions exist, some being better than others.¹⁷ In our first IOP experiments¹⁵ we used a $3N$ -element linear input LED array to represent the complex-valued vector \tilde{a} , with a_0 input to the first N elements, a_1 to the second N elements and a_2 to the last N elements. For the mask \underline{H} , we used a $3M \times 3M$ mask with its elements arranged as

$$\tilde{\underline{H}} = \begin{bmatrix} \underline{H}_0 & \underline{H}_1 & \underline{H}_2 \\ \underline{H}_2 & \underline{H}_0 & \underline{H}_1 \\ \underline{H}_1 & \underline{H}_2 & \underline{H}_0 \end{bmatrix}, \quad (10)$$

where each \underline{H}_i is a $M \times N$ matrix. This increased the required space-bandwidth product (SBWP) of the mask by a factor of 9. Due to limited SBWP in the current IOP, we employ the bipolar algorithm in Eq. (8) and realize the operation on complex-valued data using Eq. (5).

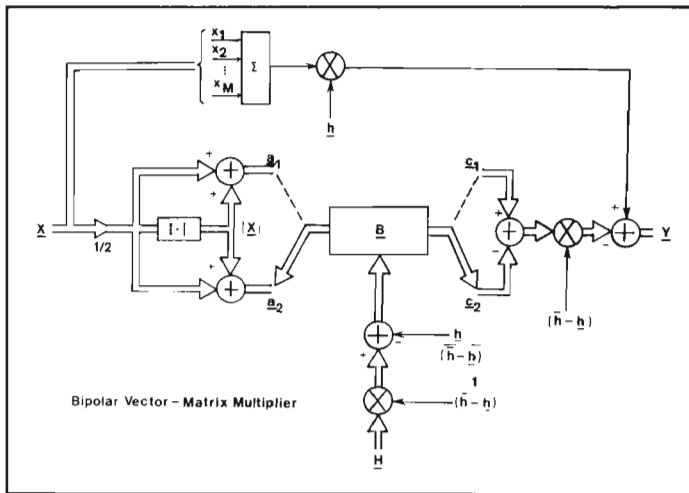


Fig. 2. Schematic diagram of a bipolar vector-matrix processor.

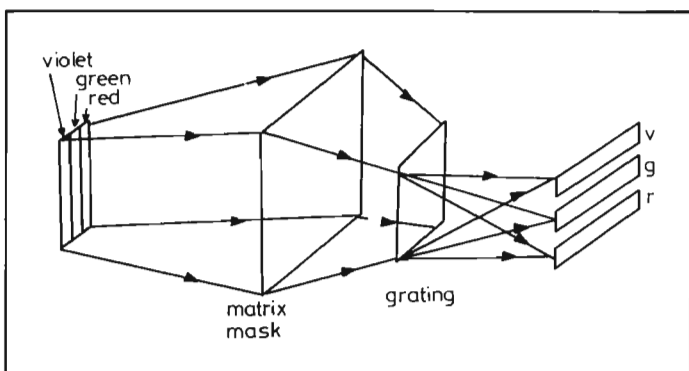


Fig. 3. Schematic diagram of a wavelength diversity processor (WDP).¹⁷

In Ref. 15, we suggested an alternative iterative vector-matrix processor for operating on complex-valued data using the decomposition in Eq. (9). This wavelength diversity processor (WDP) is shown schematically in Fig. 3. In this system, three linear laser diode arrays at the input, each with M elements and each emitting at a different wavelength λ_1 , λ_2 , and λ_3 , are used. (For the laboratory experiments performed, we used an arc lamp light source and its violet, green and orange or red output lines). We then input the three components \underline{a}_1 , \underline{a}_2 , and \underline{a}_3 of $\underline{\tilde{a}}$ to the three laser diode arrays as in Eq. (9). Each laser diode array is imaged vertically and expanded horizontally to illuminate the mask on which \underline{H} is recorded as in Eq. (10). Behind the mask we place a grating which diffracts the light leaving the mask onto three linear output detector arrays (each with N elements). On these three photodetector arrays, the product of the matrix mask and one of the input vectors at a given wavelength is formed. After properly combining the outputs from these three detector arrays, the three input vectors for the next iteration are obtained.

Figure 4 illustrates the inputs (Fig. 4(a)), mask outputs (Fig. 4(b)), and the outputs on the three linear photodetector arrays (Fig. 4(c)) obtained on the laboratory WDP system. Since Fig. 4 is printed in black and white, we denote the colors of the different light patterns by the corresponding letters: v = violet, g = green, and o = orange. For the example shown, the input vector $\underline{\tilde{a}}$ had components $a_{m1} = (1,0)$, $a_{m2} = (1,1)$ and $a_{m3} = (0,1)$ modulated on wavelengths λ_1 , λ_2 , and λ_3 respectively. The matrix mask used was 2×6 . The three outputs in three different wavelengths obtained on the detector arrays can be verified to be the correct $3 \times 6 = 18$ possible cross products expected from the system.¹⁵

We have developed additional variations of the basic WDP

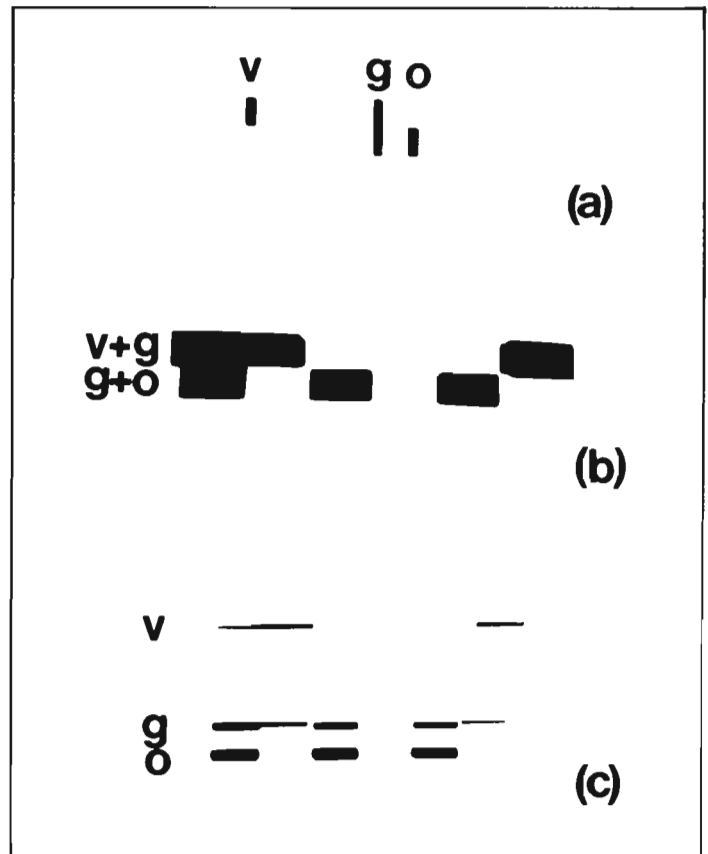


Fig. 4. Example of the multiplication of complex-valued vectors and matrices on the WDP system of Fig. 3. (a) input, (b) light distribution leaving the mask, (c) photodetector outputs.¹⁷

system of Fig. 3 with reduced mask space-bandwidth product requirements and decreased postprocessing complexity. However, the lack of commercially available linear laser diode input arrays makes these WDP systems less attractive for present fabrication. With expected technological advances, such source arrays will become available, and the WDP system will be more realistic. For now, we only note the potential use of this system and in the remaining sections concentrate our attention on the standard (monochromatic) IOP of Fig. 1.

4. CONVERGENCE OF THE ITERATIVE ALGORITHM

We now consider the convergence of the Richardson algorithm in Eq. (2). This requires attention to the selection of the acceleration factor ω in Fig. 1. First rewrite Eq. (2) as the system of first-order linear difference equations

$$\underline{x}(j+1) = [\underline{I} - \omega \underline{H}] \underline{x}(j) + \omega \underline{y}, \quad (11)$$

where \underline{I} is the identity matrix and the matrix of the homogeneous part of this difference equation is $[\underline{I} - \omega \underline{H}]$. For Eq. (2) or Eq. (11) to converge, the eigenvalues λ'_i of the system matrix $[\underline{I} - \omega \underline{H}]$ must satisfy $0 < |\lambda'_i| < 1$. We denote the eigenvalues of \underline{H} by λ_i and note that $\lambda'_i = 1 - \omega \lambda_i$; thus, for convergence we require

$$|1 - \omega \lambda_i| < 1. \quad (12)$$

In the vector-matrix applications considered, the λ_i all lie in the open left-half of the s -plane and thus have negative real parts for optimal control problems. For radar problems, the mask is the covariance matrix (which is positive-definite Hermetian); thus, its eigenvalues λ_i are real-positive numbers.

To satisfy Eq. (12), one choice for ω is

$$\omega = 1/\lambda_{\max}, \quad (13)$$

where λ_{\max} is the absolute value of the largest eigenvalue of \underline{H} . With this choice, we insure that Eq. (12) is satisfied for the largest λ_i . For smaller λ_i , it is also satisfied. In practice, ω is slightly decreased from Eq. (13) to insure that $1 - \omega\lambda_i$ is not less than zero which would cause the system to oscillate.

In Sec. 6, we describe an iterative algorithm¹⁸ to estimate λ_{\max} using the IOP. The value of ω used in the laboratory IOP is computed much more easily by using the conservative upper-bound for λ_{\max} ¹⁹

$$\lambda_{\max} \leq \|\underline{H}\| = \left[\sum_m \sum_n h_{mn}^2 \right]^{1/2}. \quad (14)$$

Since it is quite fast and easy to compute the Euclidean norm of \underline{H} as in Eq. (14), we use our microprocessor system to perform this computation once and use the value of ω so calculated in Eq. (2) or Eq. (11). This technique has been found to be applicable for all cases thus far addressed.

5. SYSTEM FABRICATION

A major concern with any optical processor is its accuracy. This factor greatly affected the design and implementation of the laboratory IOP system we fabricated. In our first IOP²⁰, we used cylindrical lenses to achieve the desired imaging between planes P_1 and P_2 and planes P_2 and P_3 of Fig. 1. In our experimental analysis of this system, we found crosstalk between the mask and nonuniform illumination of a given row of the mask to be the major errors affecting the performance of this initial IOP system. We then fabricated a new IOP in which the required imaging between P_1 and P_2 was performed using fiber optics. This greatly decreased the size and weight of the system and greatly reduced system errors (we will quantify this later in the section). Similar experimental problems were encountered in the imaging system used between P_2 and P_3 . To alleviate this latter problem, the height of the matrix mask at P_2 was selected such that it matched the height of a photodetector element at P_3 . The photodetector and mask planes were then placed in contact and all optics between them were thus avoided.

To decrease the necessary input drive electronics, the input data to the LEDs were multiplexed. Measurements of the drive for the LEDs versus their output light intensity showed a large non-linearity, especially at low current levels. In our laboratory IOP, we utilized pulsewidth modulation (PWM) of the LED outputs, a 1 MHz clock rate, a 1 μ sec minimum pulse duration and a 256 μ sec maximum pulse duration (corresponding to an input dynamic range of 256:1). This input data dynamic range is adequate for all applications with which we are presently concerned. The laboratory system assembled uses 10 LEDs, a 10×10 mask, and 10 output detector elements. Increased system dynamic range is possible either by increasing the number of pulse slots available in the PWM scheme, by electronically correcting for the nonlinear response of the LEDs, or by replacing the present sources with laser diodes (using amplitude modulation). One computational cycle of the current system requires $10 \times 0.25 = 2.5$ ms (maximum) to complete. Increased speed will result by use of individual drivers for each source, use of amplitude modulation rather than pulsewidth modulation, and a higher clock frequency (modulation of laser diodes beyond 1 GHz is possible, and a linear array of such sources is feasible if electronic crosstalk can be reduced). A photograph showing the LED sources (right), the fiber optic interconnections, mask, output detector, and detector board (left) is given in Fig. 5. (In practice, the mask, detector, and fiber optic elements are in physical contact, and were separated only to better show each component. The actual system is less than five inches long.)

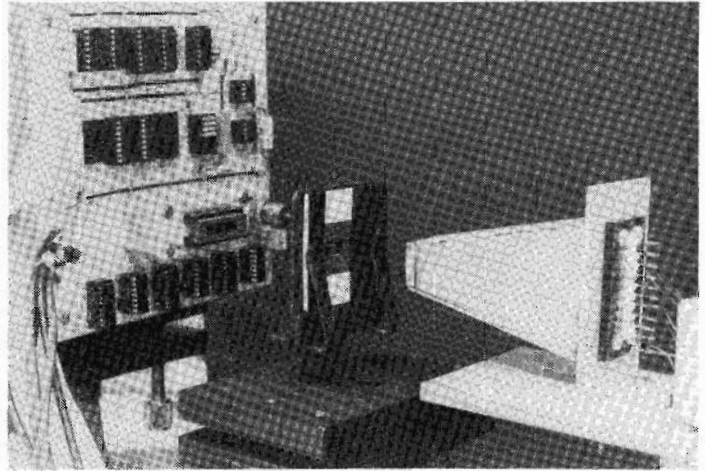


Fig. 5. Photograph of the components of the laboratory iterative optical processor (IOP).

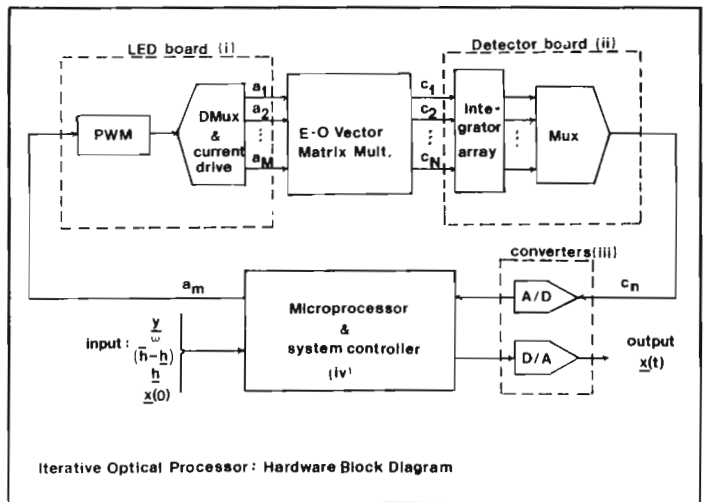


Fig. 6. Hardware block diagram of the iterative optical processor (IOP) microprocessor based system.

The purpose of the laboratory assembled IOP system was not to achieve the maximum possible state of the art in speed, size, and dynamic range, rather it was fabricated to uncover unforeseen problems in future designs of such systems as well as to determine and verify the accuracy possible from such a system and to isolate future component work required.

A schematic of the IOP emphasizing the microprocessor electronic support system is shown in Fig. 6. To maintain flexibility in the applications for which the IOP can be used, the fixed external vector is added in hardware (it could be done optically by appending an extra row to the mask and illuminating it with a second linear LED array), and corrections for LED and photodetector response differences are achieved by using a 16-bit 300 nsec multiplier to multiply the respective inputs and outputs by the response correction factors stored in a random access memory (RAM). The electronic feedback support system also includes a 16-bit arithmetic logic unit (ALU) and 16k RAM, plus a 26k RAM (for storage of microprograms), a Fairchild 9408 LSI microprogram sequencer, and a 32 line instruction decoder. This system performs all of the necessary scaling, biasing, bipolar postprocessing, computation of the acceleration parameter ω from the norm of \underline{H} , plus the necessary sequencing, control, multiplexing, and demultiplexing required. A memory system is also included to allow storage of up to 64 successive output iterations from the system for subsequent display on an oscilloscope or for input to a minicomputer for

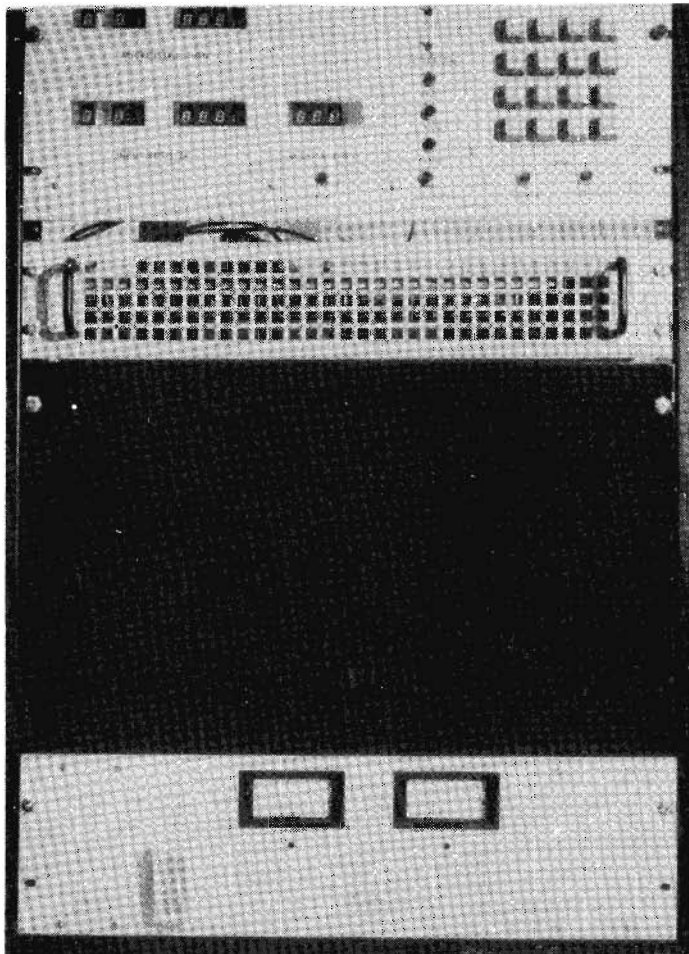


Fig. 7. Photograph of the full iterative optical processor (IOP) system including front panel, power supplies, microprocessor system and the optical processor.

future analysis. A photograph of the entire IOP system is shown in Fig. 7. It contains a front panel (to allow operator control of the system), the entire microprocessor system, all necessary power supplies, and the IOP itself (behind the dark lower panel).

In the laboratory system assembled, the spatial nonuniformity of the saturation levels of the LEDs used was measured to be 25%. This was corrected by multiplying the inputs to the LEDs by the appropriate fixed correction factors stored in RAM. The spatial nonuniformity and the response of the photodetectors was measured to be $\pm 7\%$. This was similarly corrected by multiplying each photodetector's output by the reciprocal of its response at half of saturation. When these major component error sources were corrected for, the system's residual 2-D spatial nonuniformity (due to LED coupling errors, fiber optic nonuniformity, and mask nonuniformity) was measured to be less than 0.8%. This fixed spatial nonuniformity can be reduced even further by placing a fixed correction mask in contact with the mask at P_2 . Because better than 1% accuracy was available from the system, we chose not to use a correction mask for the initial research. As noted earlier, all fixed pattern detector noise is cancelled by the bipolar algorithm of Eq. (8). The major error sources remaining in the system are thus the time-varying detector noise (we measured this to be 0.1%) and noise errors in the data recorded on the mask itself. We are presently analyzing these error sources and their effect on the system's output in selected applications by digital simulation and experiment.

6. APPLICATIONS

We have considered diverse applications for the IOP and have

demonstrated many of them. The original motivation for this system was as a processor for an adaptive phased array radar.²⁰ In this application, the external vector input \underline{y} is the steering vector \underline{s} (that describes the direction in which we wish to steer the antenna), the matrix \underline{H} is the covariance matrix \underline{M} that describes the antenna's far-field noise distribution, and the vector \underline{x} is the set of adaptive weights \underline{w} we wish to determine. When the weights \underline{w} are applied to the antenna's received signals, the antenna is steered in the direction defined by \underline{s} and the entire noise field pattern in other directions (defined by \underline{M}) is nulled. In this application, the elements of the vectors and matrices are complex-valued. We have used the input vector format in Eq. (9) and the matrix format in Eq. (10) to describe and handle such data^{15,20} as well as the techniques in Eqs. (5) and (8).¹⁸

We have also applied the IOP to optimal control applications including solution of the linear quadratic regulator and algebraic Riccati equations. In this application,²¹ the solution of nonlinear matrix equations is required. We accommodate this by vectorization of the matrices. Because of the nonlinear matrix-matrix equations involved, we utilize two iterative loops in the system: an inner iterative loop is used to compute the next iterative input for an outer iterative loop. In each outer loop iteration, the matrix at P_2 must be changed. We plan to achieve this by using a real-time CCD-addressed spatial light modulator such as the liquid crystal light valve²² at P_2 in future versions of this system.

We have successfully demonstrated the use of the IOP for inverse filtering and matrix inversion and have formulated its use for Wiener filtering. For matrix inversion, we describe the IOP by $\underline{Y} = \underline{M}\underline{X}$, where all quantities are matrices. In practice, \underline{Y} and \underline{X} are lexicographically-ordered vectors, and \underline{M} is a specially formatted matrix. Alternatively, each column of \underline{X} can be sequentially input to the system. When the external vectors are added the columns of the identity matrix \underline{I} , the system's output \underline{x} or \underline{X} is the desired inverted matrix \underline{M}^{-1} in the steady state.

We have likewise used the system to compute the eigenvalues and eigenvectors of a matrix. In these applications, we describe the initial input $\underline{x}(0)$ at iteration zero by a vector that is a linear combination of the eigenvectors $\underline{\phi}_m$ to be computed, i.e.,

$$\underline{x}(0) = a_1\underline{\phi}_1 + a_2\underline{\phi}_2 + \dots + a_M\underline{\phi}_M. \quad (15)$$

After k iterations, with the output sent directly back to the input, without adding a vector \underline{y} we find

$$\underline{x}(j) = \underline{H}^j \underline{x}(0). \quad (16)$$

By singular-value decomposition²³ in terms of the eigenvalues λ_m and eigenvectors $\underline{\phi}_m$ of \underline{H} ,

$$\underline{H} = \sum_m \underline{\phi}_m^+ \lambda_m \underline{\phi}_m. \quad (17)$$

Combining Eqs. (15) to (17), we find $a_m = \underline{\phi}_m^T \underline{x}(0)$, and Eq. (16) can be written as

$$\underline{x}(j) = \sum_m \underline{\phi}_m \lambda_m^j a_m. \quad (18)$$

After a sufficiently large number j of iterations, the eigenvector $\underline{\phi}_d$ with the largest eigenvalue λ_{\max} will dominate the summation in Eq. (18) and thus Eq. (18) can be approximated by

$$\underline{x}(j) \approx \underline{\phi}_d \lambda_{\max}^j a_d. \quad (19)$$

From the ratio $\underline{x}(j+1)/\underline{x}(j)$, we can determine λ_{\max} . It is also possible to extend this conventional power method²⁴ to allow computation of all of the eigenvalues and eigenvectors of \underline{H} .^{25,26}

7. CONCLUSIONS

Many problems can be expressed as vector-matrix and matrix-matrix equations. The selected examples briefly described in Sec. 6 were included to show the potential of this IOP system as a general-purpose processor. The improvements in LED and laser diode sources and in fiber optic technology that will result from the present interest in the communications industry will serve to provide adequate components for advanced IOP systems. It is difficult to speculate on the potential processing capacity of the IOP, however, 500 input laser diodes and a 500×500 element mask are certainly possible, as are 1 GHz detectors and light sources. With such components, computation rates of over 10^{16} bipolar multiplications and additions per second are possible on this system. Even if the final system has a performance of 100 or 1000 times below this optimistic value, this type of optical processing architecture still offers considerable size, weight, cost, and computing advantages over many other technologies. For these reasons, it is expected that optical matrix-vector processors will be major candidates for advanced data processing applications.

ACKNOWLEDGMENTS

We thank NASA-Lewis Research Center (Grant NAG-3-5) for present support of this research and the Air Force Office of Scientific Research (Grant AFOSR 79-0091) for interim support of this data processing concept.

REFERENCES

1. J. W. Goodman, "Operations achievable with coherent optical information processing systems," Proc. IEEE 65, 29 (1977).
2. A. Huang, Y. Tsunoda, J. W. Goodman, and S. Ishihara, "Optical computation using residue arithmetic," Appl. Opt. 18, 149 (1979).
3. D. Psaltis and D. Casasent, "Optical residue arithmetic: a correlation approach," Appl. Opt. 18, 163 (1979).
4. Section on Numerical Optical Processing in 1980 *International Optical Computing Conference (Book II)*, W. T. Rhodes, ed., Proc. SPIE 232, 109-174 (1980).
5. J. Trimble, D. Casasent, D. Psaltis, M. Carlotto, and D. Neft, "Digital correlation by optical convolution/correlation" in *Real-Time Signal Processing III*, T. F. Tao, ed., Proc. SPIE 241, 155 (1980).
6. L. Cutrona, "Recent Developments in Coherent Optical Technology," in *Optical and Electro-Optical Information Processing*, J. Tippett et al., eds. (MIT Press, Cambridge, 1965).
7. P. Mengert and T. Tanimoto, U.S. Patent No. 3,525,856, filed 6 October 1966.
8. A. Edison and M. Noble, Final Report, Contract AF19 (628-4199) General Electric Company (November 1966).
9. M. Monahan, R. Bocker, K. Bromley, and A. Louie, "Incoherent electro-optical processing with CCD's," in *International Optical Computing Conference 1975* (April 1975; IEEE Order No. 75-CH0941-5C), pp. 25-33.
10. M. Monahan, K. Bromley, and R. Bocker, "Incoherent optical correlators," Proc. IEEE 65, 121 (1977).
11. J. W. Goodman, A. R. Dias, and L. M. Woody, "Fully parallel, high-speed incoherent optical method for performing discrete Fourier transforms," Opt. Lett. 2, 1 (1978).
12. J. W. Goodman, A. R. Dias, L. M. Woody, and J. Erickson, *Incoherent Optical Matrix-Vector Multiplier*, Stanford University Technical Report No. L-723-1 (February 1979).
13. J. W. Goodman and L. M. Woody, "Method for performing complex-valued linear operations on complex-valued data using incoherent light," Appl. Opt. 16, 2611 (1977).
14. J. W. Goodman, A. R. Dias, K. Johnson, and D. Peri, "Parallel incoherent optical matrix-vector multipliers," in *Workshop on Future Directions in Optical Information Processing*, J. Walkup and T. Krile, eds., Texas Tech University, Final Report on ARO Contract DAAG 29-80-C-0110 (May 1980), pp. 116-126.
15. D. Psaltis, D. Casasent, and M. Carlotto, "Iterative color-multiplexed, electro-optical processor," Opt. Lett. 4, 348 (1979).
16. L. F. Richardson [1910], Phil. Trans. Roy. Soc. London A210, 307-357; 159, 207, 281.
17. A. R. Dias, "Incoherent Matrix-Vector Multiplication for High-Speed Data Processing," Ph.D. Thesis, Stanford University, June 1980 (University Microfilms Order No. 80-24641, Ann Arbor, Mich.). (Also published as Stanford Electronics Laboratories Technical Report No. L722-4.)
18. M. Carlotto, "Iterative Electro-Optic Matrix Processor," Ph.D. Thesis, Carnegie-Mellon University, April 1981 (University Microfilms Order No. 81-18788, Ann Arbor, Mich.).
19. E. Kreyszig, *Advanced Engineering Mathematics* (John Wiley, New York, 1972).
20. D. Psaltis, D. Casasent, and M. Carlotto, "Iterative optical processor (IOP) for adaptive phased array radar processing," in *Real-Time Signal Processing II*, T. F. Tao, ed., Proc. SPIE 180, 114 (1979).
21. D. Casasent, C. Neuman, and M. Carlotto, "Electro-optical processor for optimal control," in *Control and Communication Technology in Laser Systems*, K. Yong, ed., Proc. SPIE 295, 176 (1981).
22. J. Grinberg, "Liquid-crystal electro-optical modulators for optical processing of two-dimensional data," in *Optics in Radar Systems*, B. Vatz, ed., Proc. SPIE 128, 153 (1977).
23. W. Pratt, *Digital Image Processing* (John Wiley, New York, 1978).
24. G. Stewart, *Introduction to Matrix Computations* (Academic Press, New York, 1973).
25. H. J. Caulfield, D. Dvornik, J. W. Goodman, and W. T. Rhodes, "Eigenvector determination by noncoherent optical methods," Appl. Opt. 20, 2263 (1981).
26. B. Kumar and D. Casasent, "Eigenvector determination by iterative optical methods," Appl. Opt. 20, 3707 (1981). ☉